ARCHIVES OF ELECTRICAL ENGINEERING VOL. 70(1), pp. 129–143 (2021)

DOI 10.24425/aee.2021.136057

Research on a novel hybrid shielding structure of magnetic coupler for inductive power transfer system

YUN RUI LIU, CHUNFANG WANG, DONGWEI XIA, RUI YUE

Qingdao University
China
e-mail: qduwcf@qdu.edu.cn

(Received: 10.05.2020, revised: 18.09.2020)

Abstract: With the development of wireless power transfer technology, more and more attention has been paid to its electromagnetic safety. In this paper, a novel hybrid shielding structure composed of the innermost fan-shaped ferrite, the interlayer nanocrystalline strip and the outermost aluminum foil is proposed to shield the electromagnetic field of the inductive power transfer system. Eight structure parameters of the proposed shielding are optimized by finite element simulation, in order to reduce the magnetic leakage of the system and improve the utilization rate of shielding materials. In addition, the proposed structure is compared with two types of typical double-layer hybrid shielding from the perspectives of the weight, the coupling coefficient and the magnetic flux leakage. Both simulation and experiment results show that the cost and weight of the proposed shield are about 60% lower than the traditional disk shield. Moreover, the shielding layer proposed in this paper can not only effectively reduce the magnetic flux leakage of the system, but also maintain a high coupling coefficient.

Key words: coupling coefficient, electromagnetic shielding, finite element simulation, optimization design, wireless power transfer

1. Introduction

Indutive power transfer (IPT) is one of the main methods of near-field wireless power transfer, which is flexible and reliable [1, 2]. In recent years, IPT has been widely used in varies applications, such as electric vehicles, household appliances, consumer electronics, and implantable medical devices [3, 4].

The key component of an IPT system is a magnetic coupler [5, 6], which works like a transformer. However, due to a large air gap between the primary and secondary, the coupling coefficient of the magnetic coupler is low and magnetic leakage is serious. Magnetic flux leak-

age not only affects the normal operation of the devices around the IPT system, but also harms human health [7, 8]. According to the safety guidelines issued by the International Commission on Non-ionizing Radiation Protection (ICNIRP) in 2010, the exposure of the public to magnetic flux density in time-varying electromagnetic fields should not exceed 27 μT [9]. Therefore, electromagnetic shielding measures must be taken to reduce the magnetic leakage of wireless power transfer systems in practical applications, while maintaining the acceptable coupling coefficient.

At present, electromagnetic field shielding methods commonly adopted in wireless power transfer systems can be divided into either active shielding or passive shielding [11, 12]. The latter is widely used for its simplicity and practicability, and is the subject of investigation in this paper. Over the years, the research on passive shielding can be classed into three categories. The first type of study uses ferromagnetic materials with high magnetic permeability and low electrical conductivity to reduce system leakage [13, 14]. This method can significantly improve the coupling coefficient and performance of the system, but the shielding effect on the system's magnetic flux leakage is not ideal [15]. The second kind of research is to shield magnetic leakage by using conductive materials with low permeability and high conductivity [16]. This method can significantly reduce the magnetic field intensity in the non-working area, but also reduce the self-inductance and mutual inductance of the coils [17]. The third type of research uses both ferromagnetic materials and conductive materials to improve the magnetic field distribution of the wireless power transfer system. And numerous shielding structures consist of these two materials have been proposed. A shielding layer consisting of metal strips and a ferrite plate was proposed and studied in [18] and [19]. The magnetic leakage of the system was suppressed by using the shielding structure of a ferrite plate and aluminum plate [20, 21]. The shielding structure of a square ferrite plate and square aluminum plate was adopted to study the influence of ferrite shapes on system performance in [22]. Authors in [23] studied the influence of the distance between ferrite bars on the coupling coefficient and output power by adopting the shielding structure of ferrite bars and an aluminum plate. This double-layer hybrid shielding combines the advantages of the two materials to make up for their shortcomings, but there are also some problems such as large size and heavy weight. Large and heavy magnetic couplers are difficult to install and costly. Especially, since the secondary of the magnetic coupler is usually installed on the used device, the one with light weight is preferred.

Consequently, based on the concept of hybrid shielding, a new shielding structure is proposed in this paper, in order to solve the problem of the existing hybrid shielding layer. The physical appearance and structure parameters describing the dimension of shielding are introduced in Section 2. On the basis of an IPT system, eight structural parameters of the proposed shield layer are optimized by finite element simulation in Section 3. In Section 4, the comparison of the two types of typical double-layer shielding is incorporated. The experimental verification is provided in Section 5. The conclusion is presented in Section 6.

2. Proposed hybrid shielding structure

The hybrid shielding structure proposed in this paper is shown in Fig. 1, which consists of the innermost fan-shaped ferrite, intermediate nanocrystalline strip and outermost aluminum foil. The ferrite sector has high permeability and forms a low reluctance loop, which can constrain the

magnetic flux path of the system, improve the coupling performance of the system, and reduce the magnetic leakage of the system. The nanocrystal strip is very thin and has high permeability, which can also improve the coupling between the transmitting and receiving coils and further reduce the flux leakage of the system. The aluminum foil has high conductivity, which will generate eddy current in the time-varying electromagnetic field to form a reverse magnetic field to offset the original magnetic field and shield the magnetic leakage of the system.

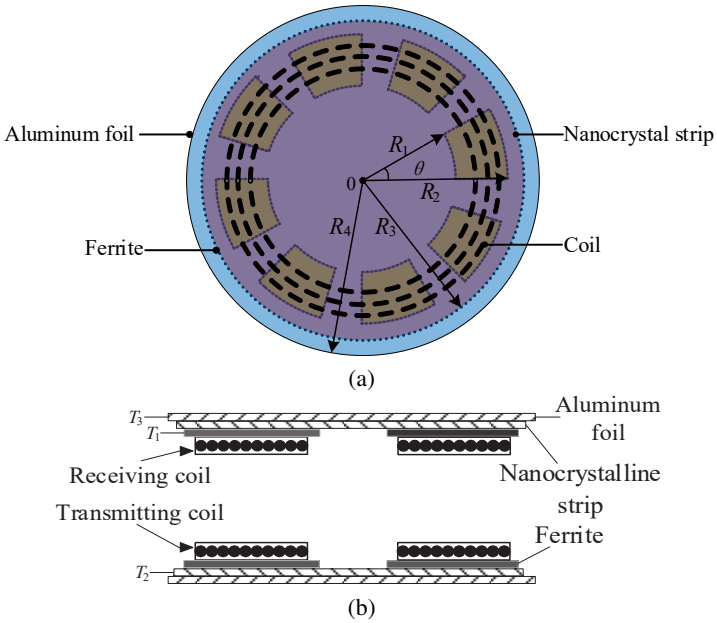

Fig. 1. Schematic diagram of the new hybrid shielding structure: (a) top view; (b) sectional view

The ferrite selected in this paper is Mn Zn ferrite with a relative permeability of 2 500 and a saturation induction of 0.5 T. The nanocrystalline adopted is FeCuNbSiB, and its thickness is 26 microns with a saturation induction of 1.2 T. The conductivity of the aluminum foil is 3.774×10^7 S·m^{-1}. The size of the Mn Zn ferrite sector is determined by its inner radius R_1, outer radius R_2, angle θ and thickness T_1. The size of the nanocrystal strip is determined by the radius R_3 and the number of layers T_2. The size of the aluminum foil is determined by its radius R_4 and thickness T_3. In order to verify the feasibility and superiority of the hybrid shielding layer proposed in this paper, the finite element simulation model of the coupler without the shielding layer is constructed in JMAG according to the actual structure and size of the coil, using the circuit simulation data of the IPT system. The transmitting coil and receiving coil of the system adopt a symmetrical circular structure with an inner radius of 30 mm and an outer radius of 53 mm. The number of turns is 12. The distance between the coils is 20 mm, and the frequency is 100 kHZ. In each case the spacing between the ferrite and coil, the nanocrystalline and ferrite, as well as the aluminum and nanocrystalline is 0.1 mm. In order to observe the magnetic leakage of the system in vertical and horizontal directions in a more detailed way, two measuring lines, as shown in Fig. 2, are selected to measure magnetic flux density.

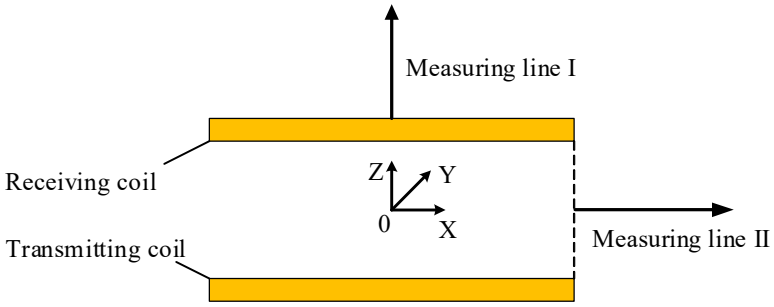

Fig. 2. Schematic diagram of measurement line

3. Optimization of the new hybrid shielding structure

3.1. Optimization of fan ferrite

Adding ferrite below the transmitting coil and above the receiving coil can constrain the magnetic flux path of the system, enhance the coupling of the system, and reduce the magnetic leakage. However, excessive use of ferrite will increase the volume, weight and cost of the system. Therefore, based on the finite element model constructed in Section 2, the four parameters of the fan-shaped ferrite are optimized to improve the system coupling coefficient and the ferrite utilization rate, aiming at increasing the coupling coefficient while minimizing the amount of ferrite. In order to compare the effects of various parameters on ferrite utilization, normalized variable URF (utilization of ferrite) is defined to characterize the utilization of ferrite, and its expression is as shown in (1).

$$\text{URF} = \frac{\Delta k}{V} 1000 \left(1/\text{c m}^3\right), \tag{1}$$

where $\Delta k = k_i - k_0$, k_i is the coupling coefficient of the system after adding ferrite; k_0 is the coupling coefficient of the system without ferrite, which is 0.36 in this paper; V is the volume of ferrite added to the system, in cm^3. According to (1), the larger the URF is, the higher the utilization rate of ferrite is. The initial parameters of the fan-shaped ferrite are as shown in (2). At this time, the coupling coefficient of the system is 0.411, the volume of the ferrite is 11.473 cm^3, and the URF is 4.15 ($1/\text{cm}^3$).

$$\begin{cases} R_1 = 25 \text{ mm} \\ R_2 = 58 \text{ mm} \\ T_1 = 1 \text{ mm} \\ \theta = 30^\circ \end{cases}. \tag{2}$$

According to the parameters shown in (2), the inner radius, outer radius and thickness of the fan-shaped ferrite are kept constant, and the angle of the fan-shaped ferrite is varied with the step of 5° for simulation analysis. The simulation results are shown in Fig. 3. As can be seen from Fig. 3, the coupling coefficient gradually increases with the increase of θ, but at the same time, the utilization rate of ferrite decreases.

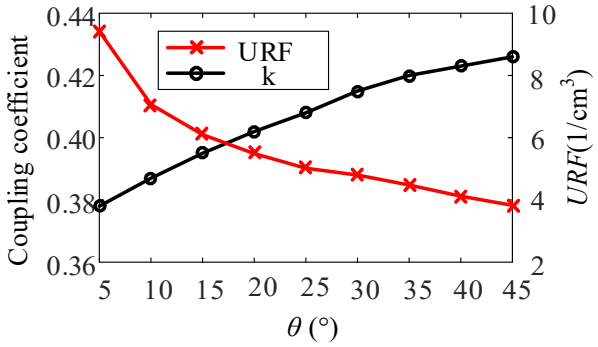

Fig. 3. Simulation results of coupling coefficient and URF versus θ

On the basis of (2), the influence of the thickness of the fan-shaped ferrite on the system coupling coefficient and ferrite utilization rate is studied. The other three parameters are kept unchanged, and only the thickness of the fan-shaped ferrite T_1 is changed for simulation analysis. The results are shown in Fig. 4. The coupling coefficient increases with the increase of thickness. Meanwhile, with the increase of the thickness of the fan-shaped ferrite, the utilization rate of the ferrite is reduced significantly, especially when the thickness is increased from 0.5 mm to 1 mm, the utilization rate is reduced by nearly 50%.

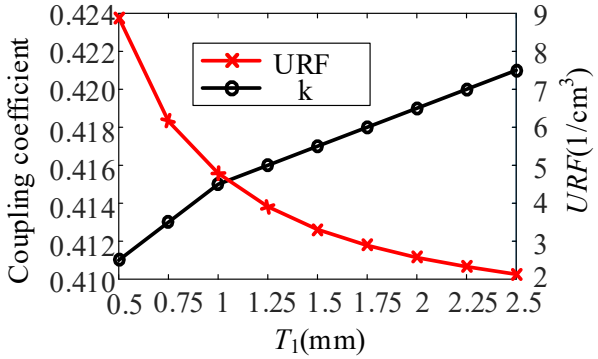

Fig. 4. Simulation results of coupling coefficient and URF versus T_1

Fig. 5 shows the influence of the fan-shaped ferrite inner radius R_1 on the system coupling coefficient and ferrite utilization rate. R_1 decreases from 50 mm to 10 mm, and the step length is 5 mm. The other three parameters of the fan-shaped ferrite are the same as those shown in (2).

It can be seen from Fig. 5, as the inner diameter decreases, the coupling coefficient of the system and the utilization rate of the ferrite increase. When the inner radius decreases from 50 mm to 20 mm, the utilization rate of the ferrite increases almost linearly.

Fig. 6 shows the profiles of the coupling coefficient and URF versus R_2R_2 is increased from 37 to 65 mm with a step of 7 mm. The other simulation parameters are identical to those given

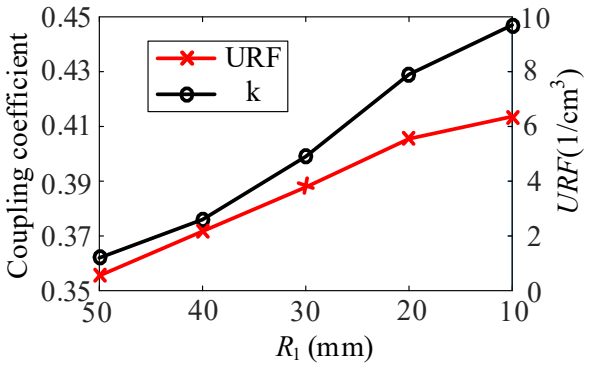

Fig. 5. Simulation results of coupling coefficient and URF versus R_1

in (2). The URF increases by 3 times, from 1.28 to 5.24, when R_2 increases from 37 to 65 mm. Moreover, the coupling coefficient also increases with the increase of R_2.

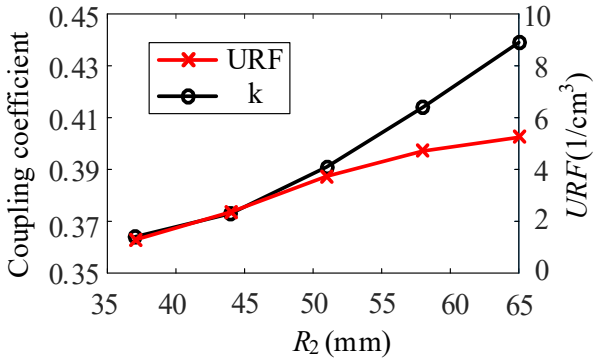

Fig. 6. Simulation results of coupling coefficient and URF versus R_2

As can be seen from the above simulation results, if any of the four parameters of the fan-shaped ferrite is changed, the coupling coefficient of the system increases with the increase of ferrite dosage, but the utilization ratio of the ferrite is different. As R_1 decreases and R_2 increases, the utilization of the ferrite gradually increases. However, the utilization rate of the ferrite decreases with the increase of T_1 and θ. Therefore, in order to increase the coupling coefficient of the system and effectively utilize the ferrite, it is possible to appropriately reduce R_1 and increase R_2 within the limits of the geometrical size. Considering the coupling coefficient of the system and the utilization ratio of the ferrite, the fan-shaped ferrite is selected with an inner radius of 20 mm, an outer radius of 58 mm, an angle of 20° and a thickness of 1 mm. Under these parameters, the coupling coefficient of the system is 0.415, URF is 4.17 (1/cm^3), and the volume of the ferrite used is 8.28 cm^3. Compared with the initial parameters shown in (2), although the system coupling coefficient and the utilization rate of the ferrite are not greatly improved, the volume of the used ferrite is reduced by 28%.

3.2. Optimization of nanocrystalline strip

On the basis of the optimized fan-shaped ferrite, a nanocrystalline strip is added to optimize its radius R_3 and number of layers T_2. Firstly, the nanocrystalline strip with the same radius as the fan-shaped ferrite is selected to study the effect of T_2 on the system coupling coefficient and vertical magnetic leakage. The simulation results are shown in Fig. 7. With the addition of nanocrystalline strips, the coupling coefficient of the system increases and the vertical flux leakage decreases significantly. However, when the number of layers of the nanocrystalline strip is greater than 2, the effect of increasing the number of layers on the system coupling coefficient and the leakage magnetic field in the vertical direction is not significant.

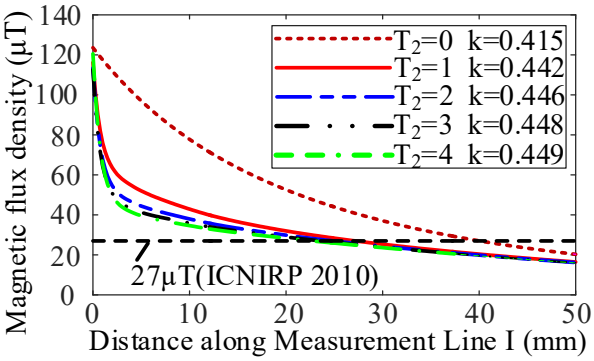

Fig. 7. Simulation results of coupling coefficient and vertical magnetic flux leakage versus T_2

Considering the influence of the number of layers of nanocrystalline strips on the coupling coefficient and vertical magnetic flux leakage, two layers of nanocrystalline strips are selected and the influence of their radius on the coupling coefficient and vertical magnetic flux leakage is further studied. The simulation results are shown in Fig. 8. As can be seen from Fig. 8, the

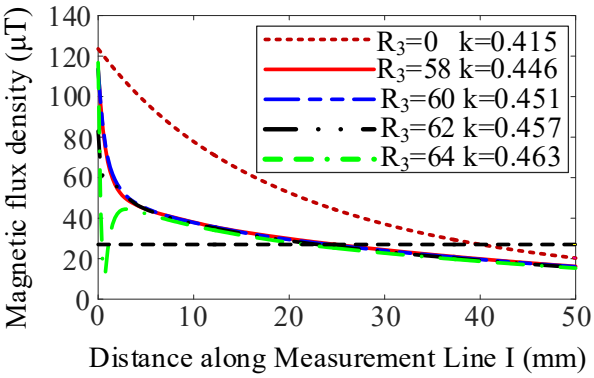

Fig. 8. Simulation results of coupling coefficient and vertical magnetic flux leakage versus R_3

coupling coefficient of the system increases with the increase of the radius of the nanocrystalline strip, which is basically linear. At the same time, although the vertical radiation distance of the system decreases with the increase of the radius of the nanocrystalline strip, the decrease is smaller and smaller. Consequently, the radius of the nanocrystalline strip is selected as 60 mm.

3.3. Optimization of aluminum foil

On the basis of the above optimized fan-shaped ferrite and nanocrystalline strip, aluminum foil is added and its parameters are optimized. Firstly, aluminum foil with a thickness of 1mm is selected to study the influence of its radius R_4 on the system coupling coefficient and horizontal magnetic flux density (magnetic flux leakage along measurement line II). The simulation results are shown in Fig. 9. As can be seen from Fig. 9, as the aluminum foil radius R_4 increases, the horizontal magnetic flux density of the system decreases faster to the human body safety limit specified by the International Commission on Non-ionizing Radiation Protection (ICNIRP). In addition, the coupling coefficient of the system decreases with the increase of the radius of the aluminum foil, but the decrease amplitude decreases with the increase of the radius. When the radius reaches 64 mm, the coupling coefficient of the system basically stops decreasing, but the horizontal magnetic flux leakage is still reducing.

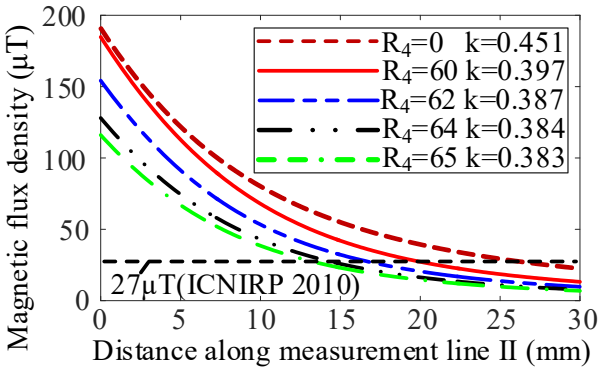

Fig. 9. Simulation results of coupling coefficient and horizontal magnetic flux leakage versus R_4

Considering the material utilization rate, system performance and system magnetic leakage comprehensively, the final values of each parameter of the new shielding layer are shown in Table 1. Under these parameters, the coupling coefficient of the system is increased by nearly 7% and the horizontal magnetic flux leakage is reduced by almost 58% compared with that without the shielding layer.

Fig. 11 shows the numerical model and finite element mesh of the optimized new shield in the computer program JMAG, where the coil is brown, ferrite is purple, nanocrystal is yellow, and aluminum foil is gray.

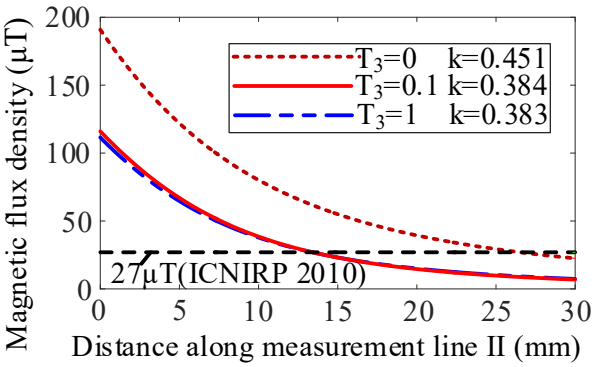

Fig. 10. Simulation results of coupling coefficient and horizontal magnetic flux leakage versus T_3

Table 1. Optimization parameters of the proposed shielding

Parameter	Description	Value
R_1	Inner radius of fan ferrite	20 mm
R_2	Outer radius of fan ferrite	58 mm
θ	Angle of fan ferrite	20°
T_1	Thickness of fan ferrite	1 mm
R_3	Radius of nanocrystalline strip	60 mm
T_2	Layers of nanocrystalline strip	2
R_4	Radius of aluminum foil	65 mm
T_3	Thickness of aluminum foil	0.1 mm

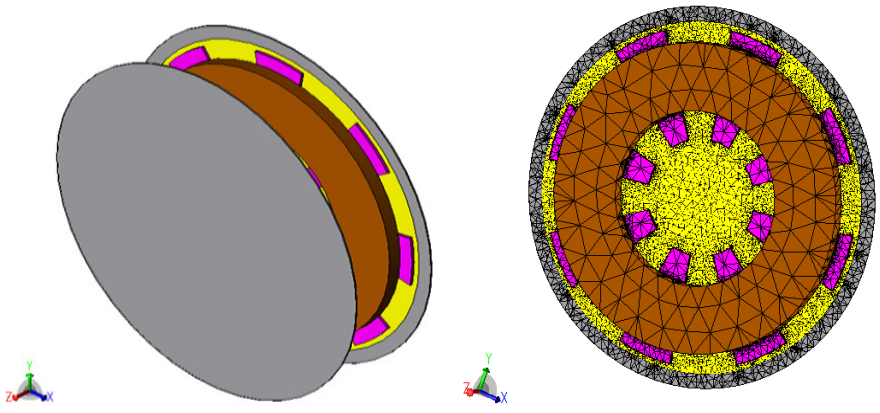

(a) (b)

Fig. 11. Finite element model of the proposed shielding: (a) 3D model; (b) finite element mesh

4. Comparison with traditional double-layer hybrid shielding

Fig. 12(a) and (b) show two typical conventional double-layer hybrid shielding structures, named a disc type shield and a strip type shield, respectively. In the figure, brown represents the coil, purple represents ferrite, and gray represents aluminum foil. By using the finite element simulation model constructed in Section 2 the new shielding layer proposed in this paper is compared with the two traditional hybrid shielding layers from three aspects, respectively, such as the shielding layer weight, the lifting effect on the system coupling coefficient and the shielding effect on the system magnetic leakage.

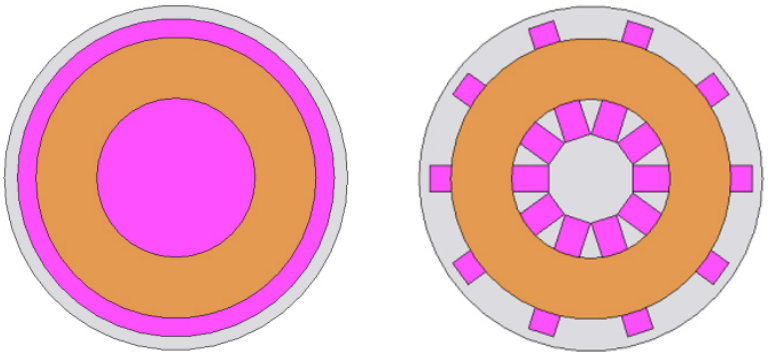

(a) (b)

Fig. 12. Traditional double-layer hybrid shielding: (a) disc type shield; (b) strip type shield

Considering that in practical application, the size of a shielding layer is limited by the application situation, the size of various shielding layers is similar. In the disc shield, the radius of ferrite is 58 mm and the thickness is 1 mm, and the radius of aluminum foil is 65 mm and the thickness is 0.1 mm. In the strip shield, the length, width and height of the ferrite strip are 45 mm, 10 mm and 1mm respectively, and the radius and thickness of the aluminum foil are 65 mm and 0.1 mm respectively. The structural parameters of the proposed shielding layer are consistent with those shown in Table 1 in Section 3.

Because the aluminum foil size of the three shielding layers is the same and the weight of the nanocrystalline strip is negligible, the volume of the ferrite is used to characterize the weight of the shielding layer. The comparison results are shown in Table 2.

Table 2. Comparison of shield weight and system coupling coefficient

Condition	**Ferrite volume (cm^3)**	**Coupling coefficient**
No shielding	0	0.36
Disc shielding	21.14	0.389
Strip shielding	9	0.337
Proposed shielding	8.28	0.384

As can be seen from Table 2 the effect of the proposed shield on the system coupling coefficient is basically the same as that of the traditional disc shield, and the weight is reduced by 60%. In addition, although the conventional strip shielding layer is equivalent in weight to the novel shielding layer proposed in this paper, the coupling coefficient, when the system adopts such a shielding layer, is even lower than that when there is no shielding. Fig. 13 shows the magnetic field distribution of the system on the ZX plane under different shielding conditions.

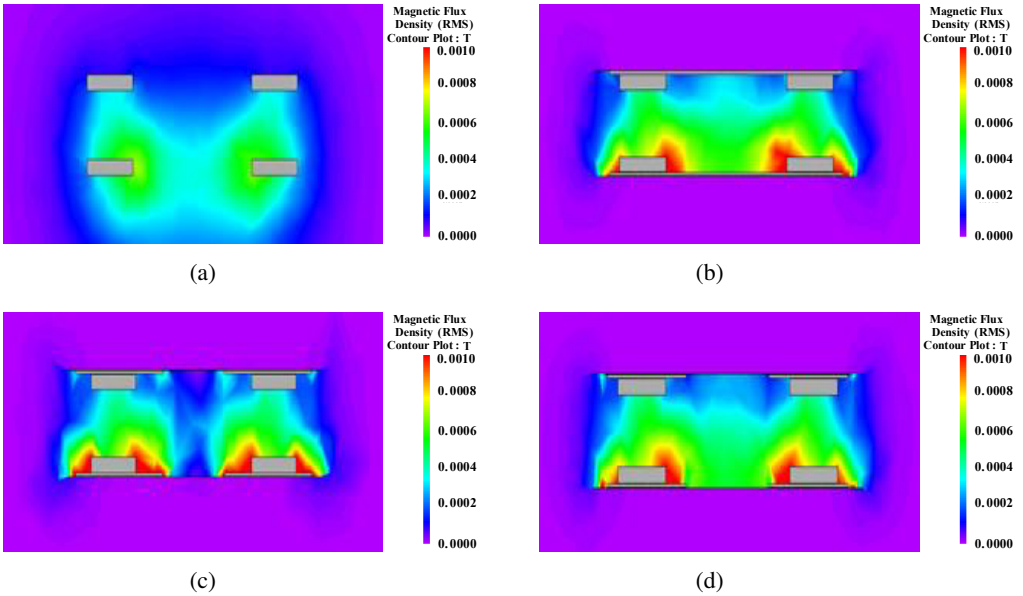

Fig. 13. Comparison of magnetic field distribution of the system with different shielding: (a) without shielding; (b) disc type shielding; (c) strip type shielding; (d) proposed shielding

It can be seen from Fig. 13, that the magnetic field of the system is more concentrated after the addition of the shielding layer than when there is no shielding layer. Moreover, the magnetic field distribution of the system using the new shielding layer is very close to that of the traditional disc shielding layer. The magnetic field in the working area is strengthened, and the magnetic field in the non-working area is weakened. The magnetic field of the working area of the system is not as strong as that of the other two types of shield, although the strip shield also allows the magnetic field of the system to be concentrated between the transmitting coil and the receiving coil.

5. Experimental verification

In order to further verify the feasibility and superiority of the new shielding layer proposed in this paper, the experimental platform shown in Fig. 14 is built for experimental verification.

Fig. 15 shows the three shielding layers used in the experiment, and the structural parameters of each shielding layer are the same as those used in Section 4.

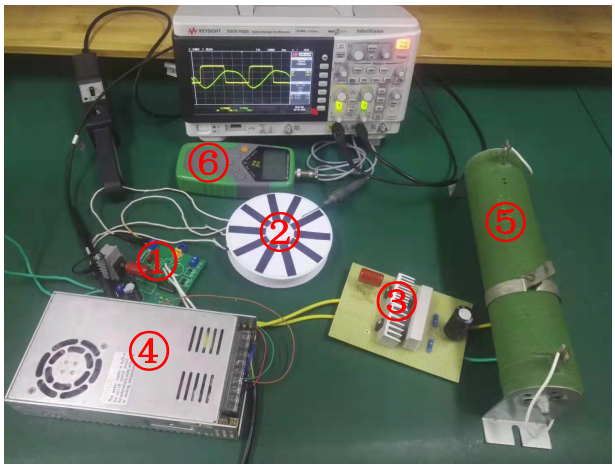

Fig. 14. Experimental platform: ① transmitting circuit; ② receiving coil; ③ receiving circuit; ④ auxiliary power supply; ⑤ load; ⑥ Tesla meter

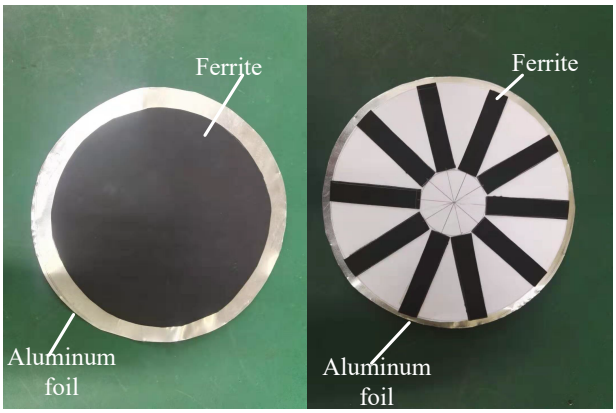

(a) (b)

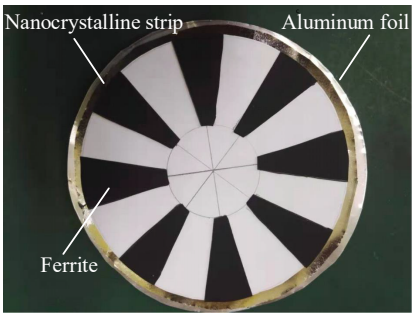

(c)

Fig. 15. Three shielding layers used in the experiment: (a) disc shield; (b) strip shield; (c) the proposed shield

The coupling coefficients of the system without a shielding layer and with three shielding layers, as shown in Fig. 15, are measured respectively. The results are shown in Table 3. It can be seen from Table 3 that the disc shielding layer has the best effect on improving the coupling coefficient of the system, but it is only about 3% higher than the proposed shielding. In addition, the coupling coefficient of the system is reduced by using a strip shield. The conclusion is consistent with the simulation analysis.

Table 3. Coupling coefficients of the system

Condition	Coupling coefficient	Promotion effect
No shielding	0.33	0
Disc shielding	0.36	9%
Strip shielding	0.31	–6%
Proposed shielding	0.35	6%

The magnetic flux leakage is measured along measurement lines I and II under different shielding conditions, and the results are shown in Fig. 16. It can be seen from Fig. 16 that the magnetic flux density along measurement lines I and II after the addition of the three types of shielding layers is substantially the same. Moreover, it is greatly reduced compared with the case of no shielding layer, which indicates that the three types of shielding layers have the similar effect on the magnetic flux leakage.

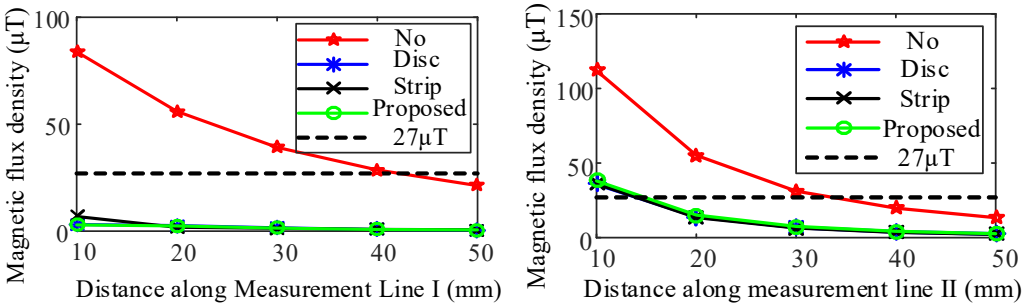

Fig. 16. Measurement of magnetic flux leakage of the system with different shielding: (a) vertical flux leakage; (b) horizontal flux leakage

6. Conclusion

This paper proposes a new hybrid shielding structure, which is light in weight and low in cost. It can reduce the flux leakage of the system and maintain a high coupling coefficient. The new shielding structure is optimized by finite element simulation, and the optimized parameters are obtained. It is compared with two types of typical double-layer shielding from three aspects.

It is found that the effects of the proposed structure on the system coupling coefficient and flux leakage shielding are nearly the same as that of the traditional disc shielding layer, and the weight is reduced by about 60%. Compared with the traditional strip shield, the coupling factor of the new shield is 12% higher and the weight is reduced by 8%. The conclusions drawn from the experiment are consistent with the results obtained from the simulation analysis, which proves the feasibility and superiority of the proposed shielding structure.

References

[1] Zhang Z., Pang H., Georgiadis A., Cecati C., *Wireless Power Transfer—An Overview*, IEEE Transactions on Industrial Electronics, vol. 66, no. 2, pp. 1044–1058 (2019).

[2] Kalwar K.A., Aamir M., Mekhilef S., *Inductively coupled power transfer (ICPT) for electric vehicle charging – A review*, Renewable and Sustainable Energy Reviews, vol. 47, pp. 462–475 (2015).

[3] Machura P., Li Q., *A critical review on wireless charging for electric vehicles*, Renewable and Sustainable Energy Reviews, vol. 104, pp. 209–234 (2019).

[4] Li H., Wang C., Liu Y., Yue R., *Research on Single-Switch Wireless Power Transfer System Based on SiC MOSFET*, IEEE Access, vol. 7, pp. 163796–163805 (2019).

[5] Zheng J., Wang C., Xia D., *Design and analysis of the ferrite air-gapped cores for a resonant inductor[J]*, Archives of Electrical Engineering, vol. 67, pp. 579–589 (2018).

[6] Xu H., Wang C., Xia D., Liu Y., *Design of Magnetic Coupler for Wireless Power Transfer*, Energies, vol. 12, no. 15 (2019).

[7] Christ A., Douglas M., Nadakuduti J., Kuster N., *Assessing Human Exposure to Electromagnetic Fields from Wireless Power Transmission Systems*, Proceedings of the IEEE, vol. 101, no. 6, pp. 1482–1493 (2013).

[8] Ding P., Bernard L., Pichon L., Razek A., *Evaluation of Electromagnetic Fields in Human Body Exposed to Wireless Inductive Charging System*, IEEE Transactions on Magnetics, vol. 50, no. 2, pp. 1037–1040 (2014).

[9] *International Commission on Non-Ionizing Radiation Protection Guidelines for limiting exposure to time-varying electric and magnetic fields (1 Hz to 100 kHz)*, Health Phys., vol. 99, pp. 818–836 (2010).

[10] Tan L., Elnail K.E.I., Ju M., Huang X., *Comparative Analysis and Design of the Shielding Techniques in WPT Systems for Charging EVs, Energies*, vol. 12, no. 11 (2019).

[11] Choi S.Y., Gu B.W., Lee S.W., Lee W.Y., Huh J., Rim C.T., *Generalized Active EMF Cancel Methods for Wireless Electric Vehicles*, IEEE Transactions on Power Electronics, vol. 29, no. 11, pp. 5770–5783 (2014).

[12] Zhu Q., Zhang Y., Guo Y., Liao C., Wang L., Wang L., *Null-Coupled Electromagnetic Field Canceling Coil for Wireless Power Transfer System*, IEEE Transactions on Transportation Electrification, vol. 3, no. 2, pp. 464–473 (2017).

[13] Zeng H., Liu Z., Hou Y., Hei T., Zhou B., *Optimization of Magnetic Core Structure for Wireless Charging Coupler*, IEEE Transactions on Magnetics, vol. 53, no. 6, pp. 1–4 (2017).

[14] Houji L., Chunfang W., Zhihao W., Dan L., *Research of shield structure for wireless power transfer system*, Advanced Technology of Electrical Engineering and Energy, vol. 38, no. 5, pp. 74–83 (2019).

[15] Stergiou C.A., Zaspalis V., *Impact of Ferrite Shield Properties on the Low-Power Inductive Power Transfer*, IEEE Transactions on Magnetics, vol. 52, no. 8, pp. 1–9 (2016).

[16] Wen F., Huang X., *Optimal Magnetic Field Shielding Method by Metallic Sheets in Wireless Power Transfer System*, Energies, vol. 9, no. 9 (2016).

[17] Li J., Huang X., Chen C., Tan L., Wang W., Guo J., *Effect of metal shielding on a wireless power transfer system*, AIP Advances, vol. 7, no. 5 (2017).

[18] Park H.H., Kwon J.H., Kwak S.I., Ahn S., *Magnetic Shielding Analysis of a Ferrite Plate with a Periodic Metal Strip*, IEEE Transactions on Magnetics, vol. 51, no. 8, pp. 18 (2015).

[19] Park H.H., Kwon J.H., Kwak S.I., Ahn S., *Effect of Air-Gap Between a Ferrite Plate and Metal Strips on Magnetic Shielding*, IEEE Transactions on Magnetics, vol. 51, no. 11, pp. 1–4 (2015).

[20] Kim H., Song C., Kim D., Jung D.H., Kim I., Kim Y., Kim J., Ahn S., Kim J., *Coil Design and Measurements of Automotive Magnetic Resonant Wireless Charging System for High-Efficiency and Low Magnetic Field Leakage*, IEEE Transactions on Microwave Theory and Techniques, vol. 64, no. 2, pp. 1–18 (2016).

[21] Kim S., Covic G.A., Boys J.T., *Tripolar Pad for Inductive Power Transfer Systems for EV Charging*, Transactions on Power Electronics, vol. 32, no. 7, pp. 5045–5057 (2017).

[22] Kim M., Byun J., Lee B.K., *Performance Analysis of Magnetic Power Pads for Inductive Power Transfer Systems with Ferrite Structure Variation*, Journal of Electrical Engineering and Technology, vol. 12, pp. 1211–1218 (2017).

[23] Budhia M., Boys J.T., Covic G.A., Huang C., *Development of a Single-Sided Flux Magnetic Coupler for Electric Vehicle IPT Charging Systems*, IEEE Transactions on Industrial Electronics, vol. 60, no. 1, pp. 318–328 (2013).